


Ex vivo assessment of basal cell carcinoma surgical margins in Mohs surgery by autofluorescence-Raman spectroscopy: A pilot study

Radu Boitor¹ | Sandeep Varma² | Ashish Sharma² | Somaia Elsheikh³ |
 Kusum Kulkarni³ | Karim Eldib³ | Richard Jerrom² | Sunita Odedra² |
 Anand Patel² | Alexey Koloydenko⁴ | Hywel Williams⁵ | Ioan Notingher¹ 

¹School of Physics and Astronomy,
 University of Nottingham,
 Nottingham, UK

²Nottingham NHS Treatment Centre,
 Nottingham University Hospitals,
 Nottingham, UK

³Department of Pathology, Nottingham
 University Hospitals NHS Trust,
 Nottingham, UK

⁴Mathematics Department, Royal
 Holloway University of London,
 Egham, UK

⁵Centre of Evidence-Based Dermatology,
 Nottingham University Hospital NHS
 Trust, Nottingham, UK

Correspondence

Ioan Notingher, School of Physics and
 Astronomy, University of Nottingha,
 University Park, Nottingham NG7 2RD,
 UK.

Email: ioan.notingher@nottingham.ac.uk

Funding information

Research for Patient Benefit Programme,
 Grant/Award Number: PB-PG-0817-
 20019

Abstract

Background: Autofluorescence (AF)-Raman spectroscopy is a technology that can detect tumour tissue in surgically excised skin specimens. The technique does not require tissue fixation, staining, labelling or sectioning, and provides quantitative diagnosis maps within 30 min.

Objectives: To explore the clinical application of AF-Raman microscopy to detect residual basal cell carcinoma (BCC) positive margins in ex vivo skin specimens excised during real-time Mohs surgery. To investigate the ability to analyse skin specimens from different parts of the head-and-neck areas and detect nodular, infiltrative and superficial BCC.

Methods: Fifty Mohs tissue layers (50 patients) were investigated: 27 split samples (two halves) and 23 full-face samples. The AF-Raman results were compared to frozen section histology, carried out intraoperatively by the Mohs surgeon and postoperatively by dermatopathologists. The latter was used as the standard of reference.

Results: The AF-Raman analysis was completed within the target time of 30 min and was able to detect all subtypes of BCC. For the split specimens, the AF-Raman analysis covered 97% of the specimen surface area and detected eight out of nine BCC positive layers (similar to Mohs surgeons). For the full-face specimens, poorer contact between tissue and cassette coverslip led to lower coverage of the specimen surface area (92%), decreasing the detection rate (four out of six positives for BCC).

Conclusions: These preliminary results, in particular for the split specimens, demonstrate the feasibility of AF-Raman microscopy for rapid assessment of Mohs layers for BCC presence. However, for full-face specimens, further work is required to improve the contact between the tissue and the coverslip to increase sensitivity.

This is an open access article under the terms of the [Creative Commons Attribution](https://creativecommons.org/licenses/by/4.0/) License, which permits use, distribution and reproduction in any medium, provided the original work is properly cited.

© 2023 The Authors. *JEADV Clinical Practice* published by John Wiley & Sons Ltd on behalf of European Academy of Dermatology and Venereology.

KEYWORDS

basal cell carcinoma, intraoperative, Mohs surgery, Raman spectroscopy

INTRODUCTION

Basal cell carcinoma (BCC) is the most common type of skin cancer, with the incidence in the United Kingdom increasing by 39% between 2000 and 2011.¹ Mohs micrographic surgery provides the highest cure rate, with the added benefit of conservation of healthy tissue as compared to wide local excision.^{2,3} During Mohs surgery, sequential thin layers of skin are removed and checked by frozen section histology to detect residual tumour, which is a process that can take 30–60 min.⁴ However, the availability of Mohs surgery is not universal because of limited capacity to process and assess histologically stained tissue sections and scarcity of specialist surgeons trained to interpret histopathology slides.⁵ Mohs surgery could be more widely adopted in practices if the surgical margins could be analysed faster and without requiring tissue processing.

Raman spectroscopy is a technique that utilises the inelastically scattered light by molecules in the sample to determine its molecular composition. Previous studies showed that Raman spectroscopy can be used to detect the endogenous molecular differences between BCC and healthy skin.^{6,7} While Raman mapping is too slow for clinical use in real time, combining Raman spectroscopy with autofluorescence (AF) microscopy decreases analysis time, allowing investigation of entire surgical margins of excised Mohs specimens intraoperatively.^{8,9} An AF image of the specimen is first captured with 405 nm laser excitation, which highlights collagen-rich connective tissue. An automated algorithm then identifies regions within this image that may be cancerous and measures the Raman spectra at these locations. The Raman spectra are then analysed using multivariate spectral classification models to provide a quantitative diagnosis (BCC yes/no) for the entire surface of the tissue.¹⁰

We have previously reported on the development and optimisation of the table-top AF-Raman prototype device.^{10,11} These studies indicated promising results on frozen skin specimens and on fresh skin specimens.^{10,11} The instrument produced repeatable results and could be operated by clinical users after only a few hours of training.

In this current study, we report the applicability of AF-Raman for intraoperative assessment of surgical margins during Mohs micrographic surgery using skin specimens from independent patients. We investigated the ability to detect the three main types of BCC (nodular, superficial and infiltrative), and evaluate the

fraction of the surgical margin area assessed during an analysis time of 30 min. The results were compared with the intraoperative assessment of Mohs surgeon and postoperative histology (the reference standard).

MATERIALS AND METHODS**Patient recruitment and specimen collection**

Fifty skin tissue specimens were obtained from 50 patients undergoing Mohs surgery at the Nottingham NUH NHS Treatment Centre. Ethical approval was granted by the Health Research Authority (HRA) and Health and Care Research Wales (HCRW) (18/WM/0105). All patients in this manuscript have given written informed consent for participation in the study and the use of their deidentified, anonymised, aggregated data and their case details (including photographs) for publication. Patients were recruited randomly at our recruitment centre, regardless of sex, age or anatomical location. Tissue layers were included in the study if their size was smaller than $2 \times 2 \text{ cm}^2$, limited by the size of the tissue cassette of the current AF-Raman prototype. If an excised layer was larger than $2 \times 2 \text{ cm}^2$, a subsection of the layer was cut to fit the cassette. Twenty-seven layers were processed and measured as split specimens and 23 layers were processed and measured as full-face specimens.

AF-Raman measurements and frozen section histology

The AF-Raman instrument (built in collaboration with RiverD International, Rotterdam, Netherlands) was integrated in the Dermatology Department at the Nottingham University Hospitals NHS Treatment Centre (Figure 1a). The specimens were excised, preprocessed and loaded in custom tissue cassettes. Sample preprocessing for AF-Raman measurements required surgeons to nick the tissue specimens to preserve orientation, immerse them in red blood cell (RBC) lysis buffer, blot them to remove superficial blood and use coloured marker pens to orientate the specimen within the cassette (Figure 1b). Excess blood was removed by immersion in 1x RBC lysis solution for 10 s, alternating with blotting the specimen between two layers of tissue

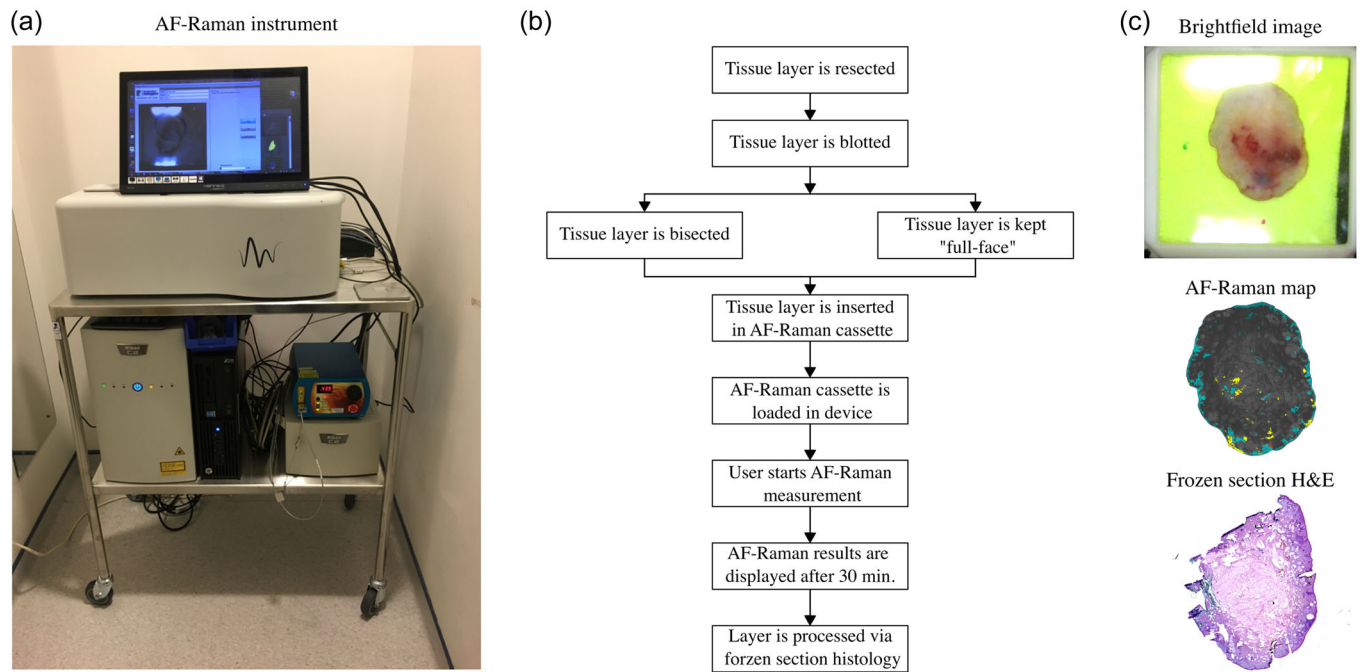
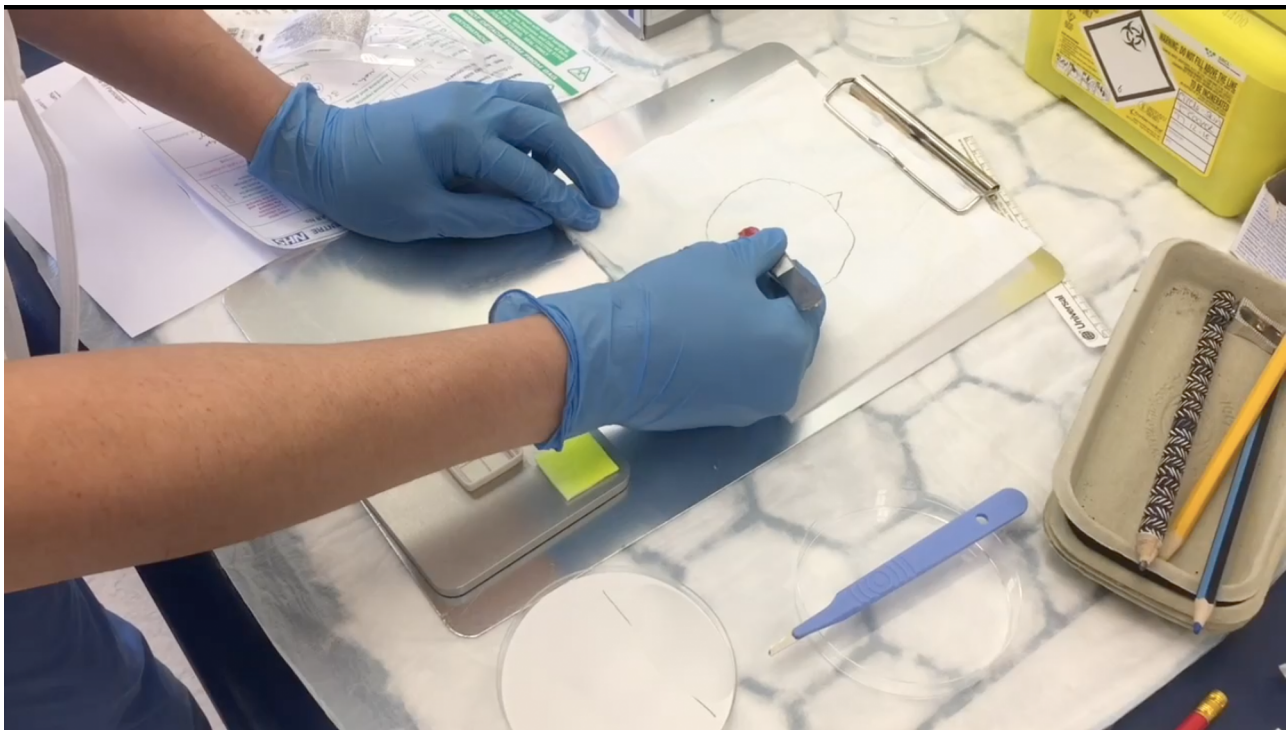


FIGURE 1 AF-Raman instrument and measurement procedure. (a) AF-Raman instrument installed at the Nottingham NUH NHS Treatment Centre; (b) flowchart of tissue processing and measurement procedure; (c) image of a typical full-face Mohs layer loaded in the AF-Raman cassette and the outputs of AF-Raman and frozen section histology. AF, autofluorescence.



VIDEO 1 Specimen preprocessing and measurement procedure for AF-Raman measurements. AF, autofluorescence.

paper. The number of blotting applications ranged from 5 to 20, depending on the quantity of blood present on the specimen, and took an average of 3 min per tissue layer and a maximum of 5 min. Tissue layers were measured

either as split specimens or as 'full-face' specimens (Figure S1). For split specimens, layers were split after blotting. The specimens were loaded in cassettes, which were inserted into the AF-Raman device (Video 1).

Measurements were started using the instrument controlling software (custom-made Matlab software). The depth of field of the instrument was defined by the optical components of the instrument to 30 μm . Therefore, the excision surface of specimens was investigated up to a depth of 30 μm . The AF-Raman analysis and diagnosis were fully automated and produced greyscale maps of the resection surface, where BCC was highlighted as red segments. The analysis time was limited to 30 min. Tissue that was outside of the 30 μm working distance from the cassette window produced low signal-to-noise Raman spectra which were identified by the device. Therefore, these regions were automatically detected and shaded in blue in the Raman map. Likewise, regions covered by blood, for which Raman bands specific to skin were swamped by Raman bands assigned to blood, were identified by the instrument software and shaded in yellow in the AF-Raman map (Figure 1c). Regions for which the AF-Raman instrument could not provide a valid result (tissue out of contact or covered by blood) were quantified for each specimen. After analysis, the specimens were inked and sent to the histopathology lab to be processed for frozen section histopathology, as per standard procedure in our Mohs unit. This consisted of pressing the tissue layer against a glass coverslip and freezing it in place while embedded in OCT (optimal cutting temperature compound). Samples were then cut with a microtome into 10 μm thick sections alongside the resection surface in 100 μm increments. The sections were stained with histopathological dyes haematoxylin and eosin. Sections were cut until the entire epidermis could be observed by the surgeon. Tissue processing for frozen section histopathology took between 30 and 60 min per tissue layer, depending on anatomical tissue and the experience of the Mohs technician.

Intraoperative assessment by Mohs surgeon and postoperative histology (reference standard)

The haematoxylin–eosin (H&E) stained frozen sections were evaluated by three assessors, blinded to each other's evaluation and the AF-Raman result. Each assessor was provided with a report form printed on A4 paper which contained the outline of the investigated tissue layer. The assessors were asked to mark the location of residual BCC with a red pen and any uncertain regions (such as inflammation or follicular structures) with a blue/black pen.

The first assessment was the routine intraoperative evaluation performed by the Mohs surgeon. Slides were

assessed with a 100 μm distance between sections. Deeper H&E sections were examined for tumour presence until the surgeon was satisfied that a full-face section of the tissue was examined. Based on the interpretation of H&E sections and various external factors (including quality of frozen sections, lesion location, patient age, etc.), the surgeon decided whether a new layer of skin needed to be excised. Any uncertainties that prompted a further resection, unrelated to BCC (such as inflammation, missing epidermis, etc.) were noted by the Mohs surgeon. If no BCC was detected, the tissue was deemed as negative (i.e., clear margins).

The reference standard for AF-Raman was postoperative histology performed on the same set of frozen section H&E slides available to the Mohs surgeon. The slides were evaluated independently by two dermatopathologists. In cases of disagreement, the two dermatopathologists reassessed the slides together, convening on a definitive diagnosis. Tissue sections were examined in the order of dissection, from the outer resection surface inward. Serial sections were examined until a full-face section was obtained (where the epidermal edge is visible in a single flat plane), unless a definite tumour deposit was detected on an earlier section. As this diagnosis was based on a concordant assessment, it was the most reliable reference for the study.

RESULTS

For the set of 27 tissue specimens split in two halves, postoperative histology identified nine layers as BCC-positive and 18 layers as BCC-negative. The split set contained five nodular BCCs, two superficial BCCs and two infiltrative BCCs. AF-Raman detected eight out of the nine BCC-positive layers, with the false negative detection being caused by a nodular BCC. From the 18 BCC-negative samples, AF-Raman provided correct results for 14 layers. For the same tissue specimens, the intraoperative assessment by the Mohs surgeons agreed with the postoperative histology assessment in eight out of nine BCC-positive cases, indicating a similar level of sensitivity as the AF-Raman instrument. However, the Mohs surgeons produced a more reliable diagnosis for the BCC clear specimens: 17 out of 18 layers.

For the set of 23 full-face specimens, postoperative histology identified six layers as BCC-positive and 17 layers as BCC-negative. The full-face set contained one nodular BCC, two superficial BCCs and three infiltrative BCCs. Out of the six BCC-positive layers, four were correctly detected by AF-Raman and two were missed (one superficial and one infiltrative). The Mohs surgeons

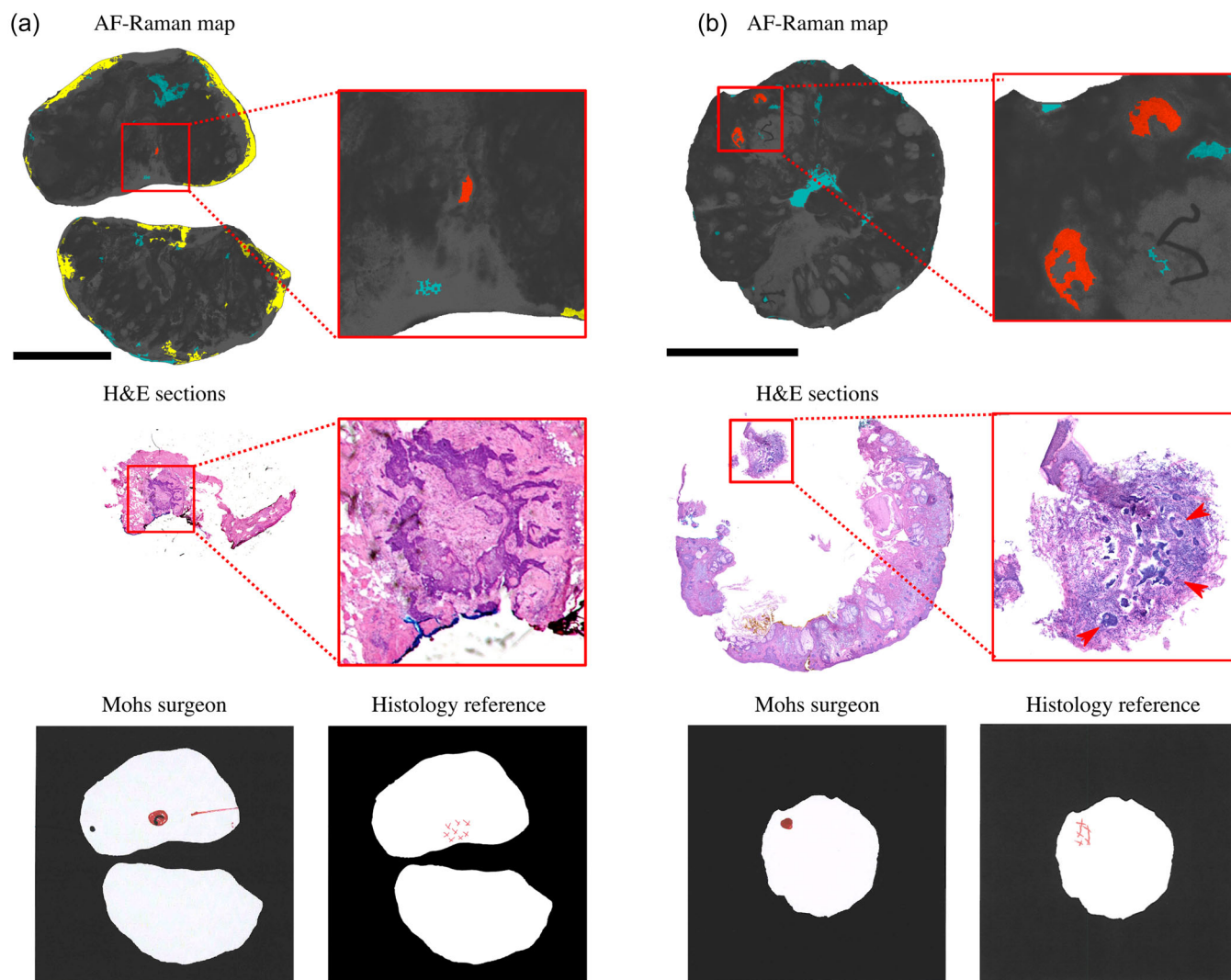


FIGURE 2 True positive AF-Raman detections according to the reference standard. (a) True positive AF-Raman detection of split layer resected from the nose; (b) true positive AF-Raman detection of full-face layer resected from the nose. BCC clusters are highlighted by red arrows in the H&E sections. The Mohs surgeon report and the histology reference report show the location where residual BCC was identified with red markers and where confounders are identified with blue markers. Scale bars: 5 mm. AF, autofluorescence; BCC, basal cell carcinoma; H&E, haematoxylin-eosin.

produced a more reliable diagnosis for the BCC positive full-face specimens, correctly identifying all six such layers. From the 17 BCC-negative full-face layers, AF-Raman provided correct results for 13 layers while the Mohs surgeon provided correct results for 14 layers.

Assessment of 100% peripheral margin was generally not possible via AF-Raman. Specimens from eyelids were investigated for 95.8%, noses for 96.7% and cheeks for 97.7% of their resection surface area. Eyelid specimens were covered in superficial blood, while stiff and thick collagen of the nose prevented these specimens from laying flat in the cassette. By comparison, 98.5% of forehead and lip margins were analysed. For full-face layers, the average analysed excision surface was ~5% lower than for split layers, due to difficulties in laying flat

the tissue specimen. While the percentage of the surface area that was covered by blood was similar between the two sets, an increase of ~5% was observed in area that was out of focus for AF-Raman measurements. This increase is caused by the saucer shape of full-face specimens and their overall thicker nature.

Two typical examples of correct BCC-positive diagnoses are presented in Figure 2, including one case of nodular (Figure 2a) and one case of infiltrative (Figure 2b) BCC. In these cases, the locations of the detected tumour matched the areas indicated by the postoperative histology and intraoperative diagnoses provided by the Mohs surgeon.

One true positive AF-Raman detection was of particular interest because both the Mohs surgeon

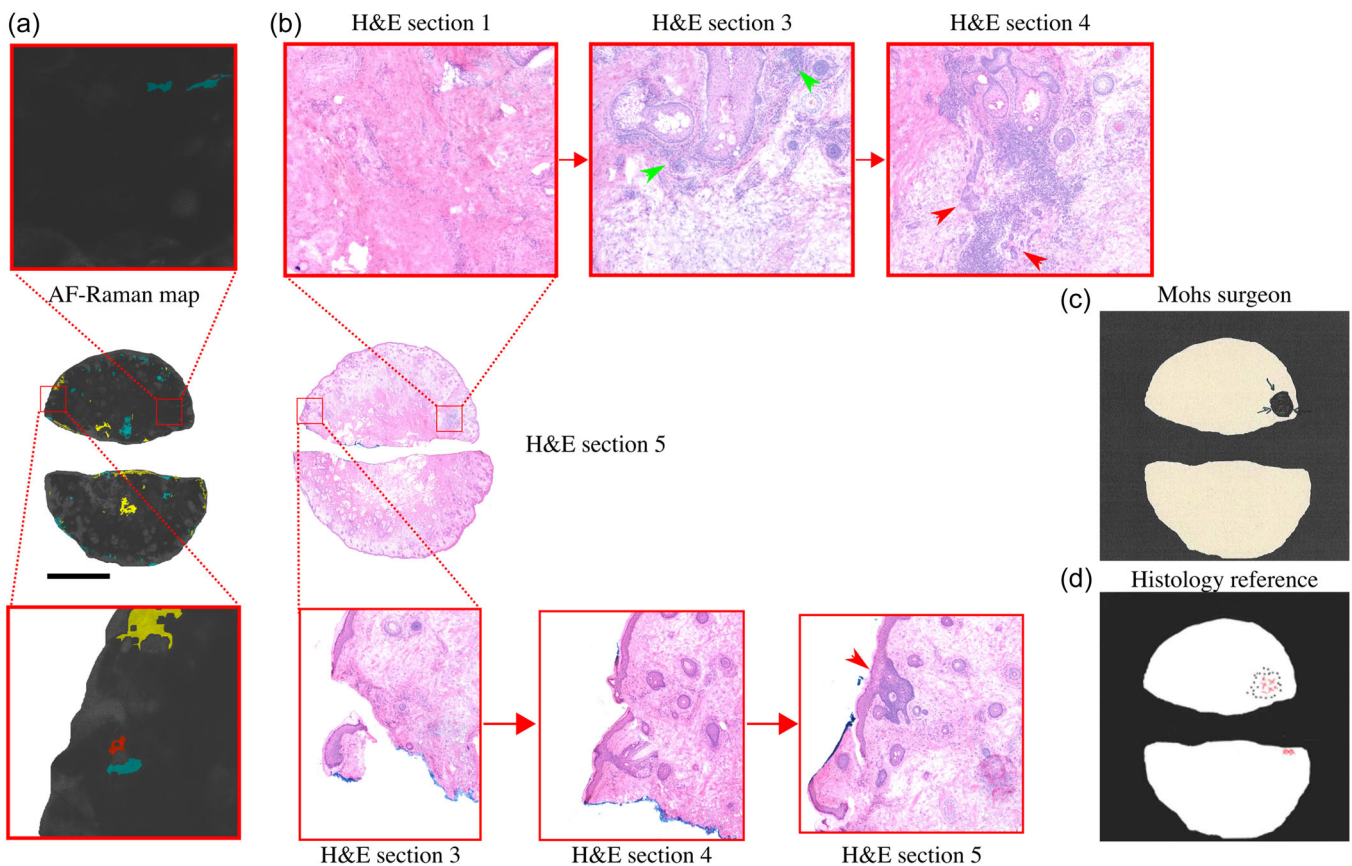


FIGURE 3 Tissue specimen (nose) that generated a true positive AF-Raman diagnosis and a false negative Mohs assessment. (a) AF-Raman map accompanied by insets highlighting the two regions of interest; (b) H&E frozen sections accompanied by insets highlighting the two regions of interest across multiple sections; (c) Mohs surgeon report form highlighting inflammation in green pen; (d) postoperative histology report form highlighting BCC in red pen. BCC clusters are highlighted by red arrows in the H&E sections. BCC confounders are highlighted by green arrows in the H&E sections. Scale bars: 5 mm. AF, autofluorescence; BCC, basal cell carcinoma; H&E, haematoxylin-eosin.

and the initial postoperative assessment disagreed with what was eventually deemed as a correct detection by consensus postoperative histology (Figure 3). The surgeon identified a region of dense inflammation on the right side of the layer (Figure 3b), which is reflected in the Mohs surgeon report in Figure 3c (green pen). While the initial postoperative histology report indicated that this area contained residual BCC (Figure 3d), consensus postoperative assessment of the slides by both histopathologists did not detect BCC in the region. Nodular BCC was only observed in this region from H&E section 4 onwards suggesting a clear margin of at least 300 μm at this location. During this assessment, the histopathologists identified a residual superficial tumour which was not observed initially on the left side of the layer. This tumour was identified by the AF-Raman analysis (Figure 3a), but was not identified by the Mohs surgeon (Figure 3c) or by the initial histopathological assessment (Figure 3d). The superficial BCC appeared in H&E section 5 (red

arrow), in the same location as a tear that was observed in H&E section 4.

The only false negative AF-Raman diagnosis in the split set is presented in Figure 4. H&E section 1 shows a small amount of inflammation and two clusters of BCC, consisting of 3–4 cells each (Figure 4b, highlighted by red arrows). Larger nodular BCC regions can be observed from H&E section 2 onwards, accompanied by inflammation (red arrows). The specimens in the data set had an average of 65 μm (up to 120 μm) of their resection surface removed by frozen section processing before the first H&E section was obtained. The surface of the sample presented in Figure 4 was trimmed (faced) by 100 μm before cryo-sectioning. Because the AF-Raman device only scans the outermost 30 μm layer of the resection surface, it may provide a more accurate representation of whether residual BCC is present in the lesion. This case shows that frozen section histology may be an imperfect standard of reference because of sparse sampling of the surface of the excised specimens.

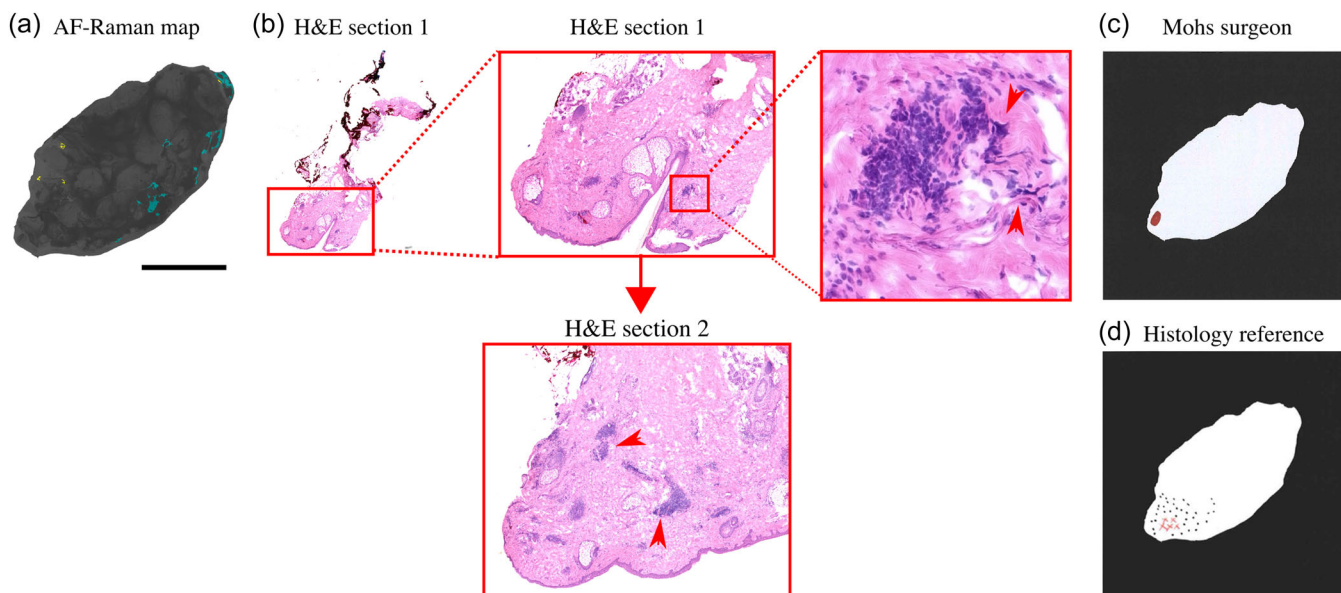


FIGURE 4 Tissue specimen (nose) that generated a false negative AF-Raman diagnosis. (a) AF-Raman map showing no red segments; (b) H&E frozen sections accompanied by insets highlighting the progression of BCC. BCC clusters are highlighted by red arrows; (c) Mohs surgeon report form highlighting residual BCC in red; (d) postoperative histology report form highlighting residual BCC in red. Scale bars: 5 mm. AF, autofluorescence; BCC, basal cell carcinoma; H&E, haematoxylin-eosin.

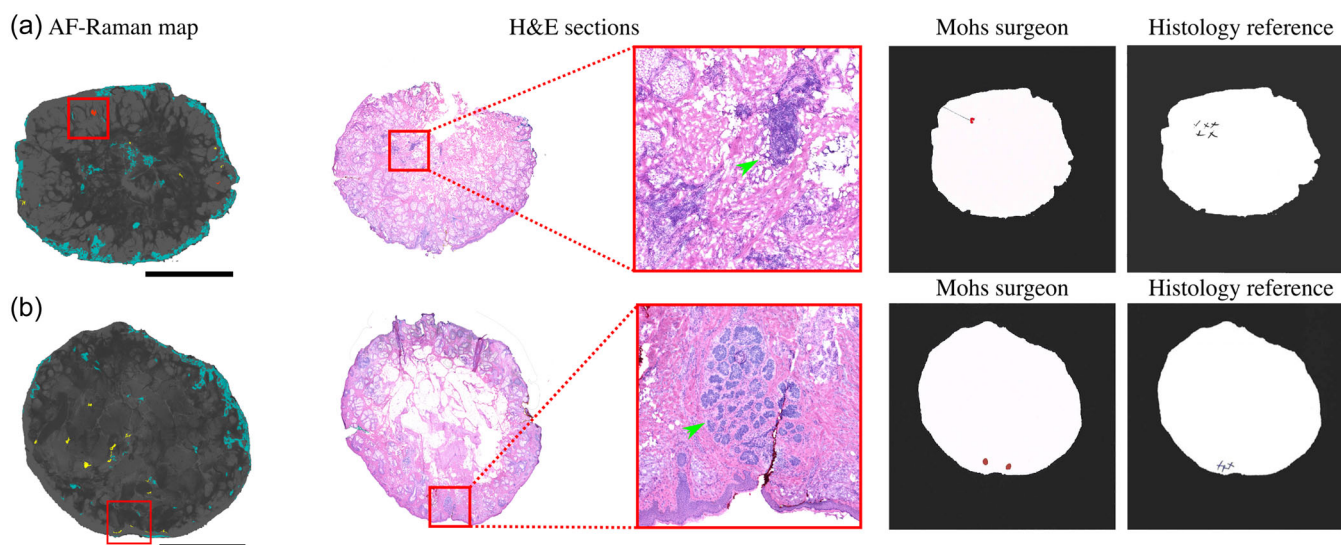


FIGURE 5 Incorrect Mohs assessments according to the histology reference standard: (a) false positive detection caused by the presence of inflammation; (b) false positive detection caused by the presence of follicular hamartoma. BCC confounders are highlighted by green arrows in the H&E sections. Incorrect residual BCC detections are marked with a red pen in the Mohs surgeon reports. BCC mimics are marked with a blue pen in the histology reference report. Scale bars: 5 mm. AF, autofluorescence; BCC, basal cell carcinoma; H&E, haematoxylin-eosin.

Four our data set, an average of $65 \mu\text{m}$ (up to $120 \mu\text{m}$) was removed and discarded from the excision surface before the first H&E section was obtained. However, because the AF-Raman scans only the outermost $30 \mu\text{m}$ layer of the excision surface, it may provide a more accurate representation of whether residual BCC is present in the lesion. However, as there is no perfect

reference standard available, the absolute truth cannot be established.

There were also two false negative AF-Raman detections in the full-face specimen set. One layer contained residual superficial BCC and one layer contained residual infiltrative BCC. The two tumours were identified by the surgeon and confirmed by

postoperative histology. For these specimens, the regions near the epidermis, where the tumours were identified, were in poor contact with the cassette window and were therefore not measured (Figure S2).

Regions incorrectly identified as BCC by AF-Raman corresponded to incipient hair follicles, sebaceous units and inflammation. False positive detections were represented as 1–2 small segments (up to 100 μm) within a layer, which were not colocalised (Figure S3). There were also a few cases where the surgeon assessment did not agree with postoperative histology (Figure 5). Figure 5a shows a tissue layer that was detected as BCC-positive by both the surgeon and the AF-Raman analysis. However, postoperative histology indicated that the detected area corresponded only to inflammation (green arrows in Figure 5a), rendering the surgeon and the AF-Raman analysis incorrect. The layer in Figure 5b is an example in which the Mohs surgeon indicated the presence of residual BCC, but postoperative histology confirmed that the observed tissue structure was a BCC mimic, more specifically, a follicular hamartoma.

DISCUSSION

This pilot study reports the first use of the AF-Raman instrument for scanning surgical margins of BCC specimens in a clinical setting, during Mohs micrographic surgery. It presents representative cases of real-world Mohs specimens being investigated by the device and outlines possible challenges in the incorporation of such a device into the clinic. The instrument had all hardware and software parameters locked at the beginning of the study and was used to analyse tissue specimens from new patients and provide diagnosis maps without any user input. For all specimens, successful measurements were reported within the 30 min target, with no detrimental effect to the tissue that could affect follow-up histology.

Preliminary results are promising, in particular for split specimens, where around 97% of the surface area was analysed. This enabled detection of the main subtypes of BCC and achieved a detection rate for BCC positive specimens comparable to that of the Mohs surgeons.

Compared to frozen section histology used in Mohs surgery, the AF-Raman has some important advantages. Tissue specimens can be scanned immediately after excision and results can be provided in a predictable time (currently 30 min). User input is limited to blotting and rinsing the specimen (up to 5 min), placing the tissue in the dedicated cassette, placing the cassette in the instrument and starting the

AF-Raman scan. The AF-Raman diagnosis map is automatically displayed after the measurement, with residual BCC highlighted in red. While AF-Raman images have a lower resolution than other emerging techniques [such as fluorescence confocal microscopy (FCM)], the resolution only needs to be sufficient to allow the surgeon to perform a follow-up resection with the expected precision required for Mohs surgery, as the AF-Raman maps do not need interpretation - residual BCC is presented in red colour. Therefore, the instrument can be used by any member of the clinical team, with minimal training of a few hours, and does not require an expert trained in optics or spectroscopy.

Several other techniques have been developed as alternatives to frozen section histology to detect residual BCC in ex vivo samples, including confocal microscopy, optical coherence tomography (OCT), two-photon fluorescence and super-pixel Raman spectroscopy.^{12–16} FCM has been shown to detect BCC with a sensitivity of 86%–92% and specificity of 60%–90%.^{17–19} These results are comparable to the results observed via AF-Raman. FCM requires fluorophores to be added to the specimen, producing grey-scale images that highlight cell nuclei and are analogous to H&E sections.^{20,21} FCM images can also be digitally coloured to appear like H&E sections,^{22,23} allowing sensitivities of 73% and specificities of 96%.¹⁸ More recently, two-photon fluorescence imaging was shown to produce real-time images of specimens up to 5 mm, which are analogous to H&E-stained sections. While this technique has not yet investigated resection surfaces, it has shown a 93% concordance with paraffin histology for a set of skin biopsies.¹⁶ Unlike AF-Raman, FCM and two-photon fluorescence require extensive tissue processing to bind fluorophores to the specimen and subjective interpretation of the images. The diagnosis is based on the identification of specific morphological features, which requires extensive training for users and can lead to variability in results.¹⁹

While the results presented in this pilot study are promising, further development is required to improve the quality of contact between tissue and cassette coverslip. This is particularly problematic for thick full-face layers that have been excised from dense collagen regions such as the nose. Inadequate measurements in poor contact regions resulted in a poor detection sensitivity. The clinical advantage of processing layers as full-face is that tissue processing for frozen sectioning takes less time (30 vs. 60 min). However, processing tissue layers as full-face also increases the number of sections needed to map the entire excision surface from an average of six for split specimens to an average of seven. Residual BCC occurrences in Mohs specimens are often found near the epidermis. In two measurements,

the low contact produced false negative diagnoses, missing superficial residual BCC.

Flattening the tissue effectively has an impact on other investigative methods, not only AF-Raman.^{17,21,23} Incomplete assessment of tissue specimens has also been reported by techniques that utilise fluorescence. Longo et al. consider an FCM image to be of good quality if the epidermis and dermal structures were recognised in at least two-thirds of the images.¹⁷ Grizzetti et al. reported that 89% of a set of FCM images (removed via Mohs surgery or slow-Mohs surgery) contained 90% or more of the tissue surface area.²³ Mu et al. excluded a third of recorded FCM submosaics due to poor image quality, related to either poor contact, inadequate staining with fluorophores or mosaic stitching artefacts.²⁴ With AF-Raman, 90% or more of the total excision surface was investigated for each layer.

Various strategies have been proposed to increase the proportion of the surface area that is analysed. For FCM imaging, additional tissue dissection, relaxing incisions and exerting pressure on the tissue specimen have been trialled.²³ Non-flat specimens can be measured repeatedly in different positions, to the detriment of measurement speed.²³ Another option is the combination of another investigative technique with a better depth of detection, such as OCT.²⁵ OCT can quickly determine the surface of the resected specimen, allowing for improved assessment by techniques which have better specificity. Combined OCT-RCM detected residual BCC with an 82.6% sensitivity and a 93.8% specificity in the surgical margin.²⁵

Additional improvements are also required to increase specificity by improving the discrimination between BCC, inflammation and incipient hair follicles. However, none of the AF-Raman false positive detections were caused by the presence of BCC mimics, such as follicular hamartoma, which were a cause of false positive detections for the Mohs surgeons. It appears that while the BCC mimics may have some common morphological features with BCC that make them difficult to discriminate from BCC by histology, they sufficiently differ in molecular composition to be correctly identified as benign by Raman spectroscopy (Figure 5).

CONCLUSION

This first pilot study demonstrates the feasibility of the AF-Raman technique for rapid assessment of fresh tissue specimens removed via Mohs micrographic surgery. It highlights the key advantages of the technique, including analysis of fresh tissue and objective diagnosis based on molecular contracts. It also indicates areas of further

developments, including the need to improve the contact between tissue and cassette coverslip. A larger study including more patients is needed to establish its diagnosis accuracy with sufficient precision. However, this preliminary study shows that the technique has the potential to extend margin-control surgery of BCC, reduce surgery time and reduce assessment subjectivity.

AUTHOR CONTRIBUTIONS

Radu Boitor, Ashish Sharma, Karim Eldib, Richard Jerrom, Sunita Odedra, Anand Patel, Kusum Kulkarni involved in the conception and design; acquisition of data, analysis and interpretation of data; drafting the article; final approval of the version to be published. In addition, Ioan Notingher, Hywel Williams, Sandeep Varma, Somaia Elsheikh and Alexey Koloydenkon led the acquisition of funding.

ACKNOWLEDGEMENTS

This manuscript presents independent research commissioned by the National Institute for Health Research (NIHR) under its Research for Patients benefit programme (grant number PB-PG-0817-20019). The views expressed are those of the author(s) and not necessarily those of the NHS or the NIHR.

CONFLICT OF INTEREST STATEMENT

S. V., A. K., H. W. and I. N. hold a patent related to Raman spectroscopy technology. The remaining authors declare no conflict of interest.

DATA AVAILABILITY STATEMENT

The data that support the findings of this study are available from the corresponding author upon reasonable request. All data recorded is available upon request from the corresponding author.

ETHICS STATEMENT

Ethical approval was granted by the Health Research Authority (HRA) and Health and Care Research Wales (HCRW) (18/WM/0105). All patients in this manuscript have given written informed consent for participation in the study and the use of their deidentified, anonymised, aggregated data and their case details (including photographs) for publication.

ORCID

Ioan Notingher  <http://orcid.org/0000-0002-5360-230X>

REFERENCES

1. British Association of Dermatology. Basal cell carcinoma. 2023. Accessed July 11, 2023. <https://www.bad.org.uk/pils/basal-cell-carcinoma>

2. Mosterd K, Krekels GA, Nieman FH, Ostertag JU, Essers BA, Dirksen CD, et al. Surgical excision versus Mohs' micrographic surgery for primary and recurrent basal-cell carcinoma of the face: a prospective randomised controlled trial with 5-years' follow-up. *Lancet Oncol.* 2008;9(12):1149–56.
3. Flohil SC, van Dorst AMJM, Nijsten T, Martino Neumann HA, Munte K. Mohs micrographic surgery for basal cell carcinomas: appropriateness of "Rotterdam" criteria and predictive factors for three or more stages. *J Eur Acad Dermatol Venereol.* 2012;27(7):907–11.
4. Shriner DL, McCoy DK, Goldberg DJ, Wagner RF. Mohs micrographic surgery. *J Am Acad Dermatol.* 1998;39(1):79–97.
5. Baxter JM, Patel AN, Varma S. Facial basal cell carcinoma. *BMJ.* 2012;345:e5342.
6. Bakker Schut TC, Caspers PJ, Puppels GJ, Nijssen A, Heule F, Neumann MHA, et al. Discriminating basal cell carcinoma from its surrounding tissue by Raman spectroscopy. *J Invest Dermatol.* 2002;119(1):64–9.
7. Larraona-Puy M, Ghita A, Zoladek A, Perkins W, Varma S, Leach IH, et al. Development of Raman microspectroscopy for automated detection and imaging of basal cell carcinoma. *J Biomed Opt.* 2009;14(5):054031.
8. Kong K, Rowlands CJ, Varma S, Perkins W, Leach IH, Koloydenko AA, et al. Diagnosis of tumors during tissue-conserving surgery with integrated autofluorescence and Raman scattering microscopy. *Proc Natl Acad Sci.* 2013;110(38):15189–94.
9. Takamori S, Kong K, Varma S, Leach I, Williams HC, Notingher I. Optimization of multimodal spectral imaging for assessment of resection margins during Mohs micrographic surgery for basal cell carcinoma. *Biomed Opt Express.* 2015;6(1):98–111.
10. Boitor R, de Wolf C, Weesie F, Shipp DW, Varma S, Veitch D, et al. Clinical integration of fast Raman spectroscopy for Mohs micrographic surgery of basal cell carcinoma. *Biomed Opt Express.* 2021;12:2015–26.
11. Boitor R, Kong K, Shipp D, Varma S, Koloydenko A, Kulkarni K, et al. Automated multimodal spectral histopathology for quantitative diagnosis of residual tumour during basal cell carcinoma surgery. *Biomed Opt Express.* 2017;8(12):5749–66.
12. Durkin JR, Fine JL, Sam H, Pugliano-Mauro M, Ho J. Imaging of Mohs micrographic surgery sections using full-field optical coherence tomography: a pilot study. *Dermatol Surg.* 2014;40(3):266–74.
13. Bennàssar A, Vilata A, Puig S, Malvey J. Ex vivo fluorescence confocal microscopy for fast evaluation of tumour margins during Mohs surgery. *Br J Dermatol.* 2014;170(2):360–5.
14. Feng X, Fox MC, Reichenberg JS, Lopes FCPS, Sebastian KR, Dunn AK, et al. Superpixel Raman spectroscopy for rapid skin cancer margin assessment. *J Biophotonics.* 2020;13(2):e201960109.
15. Atak MF, Farabi B, Navarrete-Dechent C, Rubinstein G, Rajadhyaksha M, Jain M. Confocal microscopy for diagnosis and management of cutaneous malignancies. *Diagnostics.* 2023;13:854.
16. Ching-Roa VD, Huang CZ, Ibrahim SF, Smoller BR, Giacomelli MG. Real-time analysis of skin biopsy specimens with 2-photon fluorescence microscopy. *JAMA Dermatol.* 2022;158(10):1175–82.
17. Longo C, Pampena R, Bombonato C, Gardini S, Piana S, Mirra M, et al. Diagnostic accuracy of ex vivo fluorescence confocal microscopy in Mohs surgery of basal cell carcinomas: a prospective study on 753 margins. *Br J Dermatol.* 2019;180(6):1473–80.
18. Peters N, Schubert M, Metzler G, Geppert JP, Moehrl M. Diagnostic accuracy of a new ex vivo confocal laser scanning microscope compared to H&E-stained paraffin slides for micrographic surgery of basal cell carcinoma. *J Eur Acad Dermatol Venereol: JEADV.* 2019;33(2):298–304.
19. Kose K, Fox CA, Rossi A, Jain M, Cordova M, Dusza SW, et al. An international 3-center training and reading study to assess basal cell carcinoma surgical margins with ex vivo fluorescence confocal microscopy. *J Cutan Pathol.* 2021;48:1010–9.
20. Larson B, Abeytunge S, Seltzer E, Rajadhyaksha M, Nehal K. Detection of skin cancer margins in Mohs excisions with high-speed strip mosaicing confocal microscopy: a feasibility study. *Br J Dermatol.* 2013;169(4):922–6.
21. Pérez-Anker J, Ribero S, Yélamos O, García-Herrera A, Alos L, Alejo B, et al. Basal cell carcinoma characterization using fusion ex vivo confocal microscopy: a promising change in conventional skin histopathology. *Br J Dermatol.* 2020;182(2):468–76.
22. Malvey J, Pérez-Anker J, Toll A, Pigem R, Garcia A, Alos LL, et al. Ex vivo confocal microscopy: revolution in fast pathology in dermatology. *Br J Dermatol.* 2020;183(6):1011–25.
23. Grizzetti L, Kuonen F. Ex vivo confocal microscopy for surgical margin assessment: a histology-compared study on 109 specimens. *Skin Health Dis.* 2022;2:e91.
24. Mu EW, Lewin JM, Stevenson ML, Meehan SA, Carucci JA, Gareau DS. Use of digitally stained multimodal confocal mosaic images to screen for nonmelanoma skin cancer. *JAMA Dermatol.* 2016;152(12):1335–41.
25. Aleissa S, Navarrete-Dechent C, Cordova M, Sahu A, Dusza SW, Phillips W, et al. Presurgical evaluation of basal cell carcinoma using combined reflectance confocal microscopy–optical coherence tomography: a prospective study. *J Am Acad Dermatol.* 2020;82:962–8.

SUPPORTING INFORMATION

Additional supporting information can be found online in the Supporting Information section at the end of this article.

How to cite this article: Boitor R, Varma S, Sharma A, Elsheikh S, Kulkarni K, Eldib K, et al. Ex vivo assessment of basal cell carcinoma surgical margins in Mohs surgery by autofluorescence-Raman spectroscopy: a pilot study. *JEADV Clin Pract.* 2023;1–10. <https://doi.org/10.1002/jvc2.336>